Observed Scaling in Clouds and Precipitation and Scale Incognizance in Regional to Global Atmospheric Models

Travis A. O'Brien*, Fuyu Li, and William D. Collins†

Lawrence Berkeley National Lab, Berkeley, CA, USA

†*and University of California, Berkeley, CA, USA*

Sara A. Rauscher and Todd D. Ringler

Los Alamos National Lab, Los Alamos, NM, USA

Mark Taylor

Sandia National Laboratories, Albuquerque, NM, USA

Samson M. Hagos and L. Ruby Leung

Pacific Northwest National Laboratory, Richland, WA, USA

Abstract

We use observations of robust scaling behavior in clouds and precipitation to derive constraints on how partitioning of precipitation should change with model resolution. Our analysis indicates that 90–99% of stratiform precipitation should occur in clouds that are resolvable by contemporary climate models (e.g., with 200 km or finer grid spacing). Furthermore, this resolved fraction of stratiform precipitation should increase sharply with resolution, such that effectively all stratiform precipitation should be resolvable above scales of ∼50 km. We show that the Community Atmosphere Model (CAM) and the Weather Research and Forecasting (WRF) model also exhibit the robust cloud and precipitation scaling behavior that is present in observations, yet the resolved fraction of stratiform precipitation actually decreases with increasing model resolution. A suite of experiments with multiple dynamical cores provides strong evidence that this 'scale-incognizant' behavior originates in one of the CAM4 parameterizations. An additional set of sensitivity experiments rules out both convection parameterizations, and by a process of elimination these results implicate the stratiform cloud and precipitation parameterization. Tests with the CAM5 physics package show improvements in the resolution-dependence of resolved cloud fraction and resolved stratiform precipitation fraction.

1 Introduction

As computing resources increase, climate models have been pushed to ever higher resolutions (Dennis et al., 2012b), but Williamson (2008), Li et al. (2011a), and Williamson (2012) provide recent examples of studies showing that some aspects of model climatology do not converge as resolution increases. This lack of convergence is problematic because climate change impact studies often require climatic information at the small scales characteristic of, for example, a single watershed (Kanamitsu and Kanamaru, 2007; Caldwell et al., 2009). High-resolution climate model simulations are a seemingly obvious way to provide climatic information at these scales, but non-convergent behavior (e.g., extreme precipitation that systematically increases with increasing resolution) complicates interpretation of climate change studies (Li et al., 2011a,b). Therefore it seems prudent to improve the resolution-dependent behavior of climate models to avoid such non-convergent behavior.

This non-convergent behavior has been somewhat mitigated by the standard practice of model tuning, through which model parameters are adjusted so that certain aspects of the model climatology (e.g., the top-of-atmosphere radiative balance) match observations (Hack et al., 2006). It is necessary, though perhaps unsatisfying, to adjust model parameters in this way so that the model emulates phenomena and exhibits climate sensitivities that are presumably also similar to reality, though this is not guaranteed. Murphy et al. (2004) show that the climate sensitivity of climate models is strongly controlled by the exact combination of tunable parameters. The need for scale-dependent tuning provides support for a fundamental reformulation of the processes in question so that they in fact do exhibit the appropriate behavior across scales. Further, tuning away resolution dependencies only works in the context of models with globally quasi-uniform grids. With the advent and

increasing utilization of atmospheric models with variable and adaptive meshes, this is no longer a tenable strategy.

Before endeavoring to improve resolution-dependent behavior, it is a critical prerequisite to understand exactly how model output should change with resolution. For some aspects of model climatology, the answer is obvious: there should be no change. For example, under radiative-convective equilibrium the time-mean value of the global-mean precipitation rate is constrained by global-mean tropospheric radiative divergence (Mitchell et al., 1987). Therefore, to the extent that a model maintains a constant radiative divergence as resolution changes, then the global-mean precipitation rate should not change either. However, for aspects of climatology that are inherently scale dependent, such as the variance of atmospheric state variables, clouds, and precipitation (Pressel and Collins, 2012; Kahn et al., 2011; Nastrom and Gage, 1985; Wilcox and Ramanathan, 2001; Lovejoy et al., 2008), model statistics should almost certainly depend on resolution. Observations of scale dependence are key to understanding resolution dependence in models and ultimately key to building model schemes that are properly scale-aware.

This manuscript describes an initial effort to use observations of scaling in clouds and precipitation to develop constraints on resolution-dependent cloud and precipitation behavior in atmospheric models. In Section 3, we use the observations of Wilcox and Ramanathan (2001) and Wood and Field (2011) to derive how clouds and precipitation should partition between resolved and unresolved components as resolution changes. Despite having cloud and precipitation distributions that agree well with the Wilcox and Ramanathan (2001) and Wood and Field (2011) data, we show in Sections 3 and 5 that the Community Atmosphere Model (CAM) and the Weather Research and Forecasting model (WRF) both exhibit resolution-dependent behavior that opposes the expected dependence on resolution. We define the term 'scale-incognizant' as the antonym of 'scale-aware' to describe such resolution-dependent model behavior that is either internally inconsistent or is in conflict with observed scale dependence. We examine potential causes of this dynamical core-independent, scale-incognizant behavior in Section 7.

2 Data and Methods

We use three primary sources of data in this analysis: digitized precipitation and cloud data from Wilcox and Ramanathan (2001), the global cloud-size distribution from Wood and Field (2011), and output from a number of idealized (aquaplanet) experiments with CAM (Neale et al., 2010). In Section 5, we use an additional set of aquaplanet simulations from both CAM and tropical-channel WRF (Skamarock et al., 2005); for the sake of continuity, we describe these simulations in Section 5.

2.1 Observations

We use two sets of data from Wilcox and Ramanathan (2001): the cloud number distribution (their Figure 2a), and the cloud-size dependence of precipitation intensity (their Figure 5a). Both of these sets of data are derived from two months of Tropical Rainfall Measuring Mission (TRMM) data (Kummerow et al., 1998) that is centered over the tropical Indian Ocean in the $\pm$ 20° latitude, 40°–120° longitude region. Wilcox and Ramanathan (2001) binned the original 5 by 7 km resolution TRMM data onto a $0.25° \times 0.25°$ grid for the purpose of collocating the TRMM data with top-of-atmosphere radiative flux measurements. Wilcox and Ramanathan (2001) use a clustering algorithm to identify contiguous clouds over oceanic grid cells. The cloud areas determined by the algorithm are used to derive the cloud number distribution (i.e., the number of clouds per unit area per unit size, with a given size), and the corresponding area-averaged precipitation rates are used to derive the cloud-size dependence of precipitation intensity. We use digitization software[1] to convert the graphical representation of the data presented in their manuscript to tabular form, which we use directly in the analysis presented in Section 3.

Wood and Field (2011) combine aircraft in-situ measurements of cloud sizes with data from the Moderate Resolution Imaging Spectroradiometer (MODIS) instrument onboard NASA's Terra satellite. They utilize two full years of daytime scenes (nominally 10:30 local time) at a native 1 km resolution from the MOD06 level 2 (collection 5) cloud product (Platnick et al., 2003). From each scene, they identify contiguous clouds both by the cloud chord length measured in the along-track direction of the satellite and by cloud area obtained from a recursive algorithm to cluster adjacent cloudy pixels. Wood and Field (2011) combine the MODIS cloud length estimates with aircraft in-situ measurements of cloud dimensions to show that cloud sizes are distributed as a single power law from sizes of 0.2 km to approximately 2000 km. They derive a cloud-size distribution from the MODIS cloud areas to show that this power-law dependence of cloud size is not an artifact of the cloud identification method. Wood and Field (2011) find that the cloud length distribution is well fit by the function $N(L) \sim L^{\beta} \exp[-(L/L_*)^2]$, in which the L^{β} term describes the power-law dependence and the $\exp[-(L/L_*)^2]$ term describes the rapid steepening of the power-law slope that occurs for clouds that have chord lengths larger than a scale-break at approximately $L_* =$ 2100 km. They also find that the cloud area distribution is well fit by the function $N(A) \sim A^{\beta'}$ though with a slightly steeper power-law slope, i.e., $\beta' < \beta < 0$.

[1] Engague Digitizer, which is available for free under a GNU license at http://digitizer.sourceforge.net

2.2 Model

We also use output from a set of idealized global climate model simulations from the Community Atmosphere Model version 4 (CAM4) at several different resolutions. The simulations have a prescribed SST distribution that follows the aquaplanet control experiment protocol described by Neale and Hoskins (2000). Under this protocol, all boundary conditions and atmospheric forcings are specified in a zonally and hemispherically symmetric manner such that the statistics of the resulting climate are also zonally and hemispherically symmetric. Diurnally cyclic insolation is imposed under fixed equinoctial (hemispherically symmetric) conditions. There are no radiatively active aerosols, and well-mixed greenhouse species fixed at present-day concentrations are the only radiatively active gases. Cloud condensation nuclei concentrations are set to a time-invariant, zonally-symmetric distribution appropriate for oceanic conditions. The simulations start from a state taken from a previous aqua-planet simulation. We run each simulation for six months, and we discard the first month to allow for model spin up. These CAM4 simulations are all run in atmosphere-only mode with the spectral Eulerian dynamical core (referred to hereafter simply as the 'Eulerian dycore'), with a 10 minute time step for the physics parameterizations, and with 26 vertical levels. In Section 3, we analyze four such simulations run at four different resolutions of T42, T85, T170, and T341. The T denotes triangular zonal and meridional mode truncation, and the number denotes the highest wavenumber retained in the spectral expansion of the dynamical fields. The equivalent zonal resolutions of the associated transform grid at the equator are 310 km, 156 km, 78 km, and 39 km. Model parameters, including timestep, were held constant among all the simulations, so that any difference among the simulations comes only from the difference in horizontal resolution. Table 1 lists the values of unconstrained parameters used in these simulations.

The treatment of clouds and precipitation in CAM4 is described fully by Neale et al. (2010), however we briefly summarize some relevant details here. CAM4 uses the Zhang et al. (2003) macrophysics parameterization and the Rasch and Kristjánsson (1998) microphysics parameterization. The Zhang macrophysics parameterization calculates cloud fraction, and it relates changes in this fraction to tendencies in cloud condensation and evaporation. Stratiform cloud coverage is proportional to the square root of relative humidity when relative humidity exceeds a specified threshold (91% for clouds at pressures above 750 hPa, and 70% for clouds below), and it is zero otherwise. Maximal cloud coverage of 99.9% occurs when relative humidity reaches 100%. Stratus cloud fraction, which is distinct from stratiform cloud fraction, is proportional to lower tropospheric stability. Convective cloud fraction is proportional to convective mass flux, with different coefficients of proportionality for the deep and shallow convection parameterizations. Total cloud fraction for a given grid cell is diagnosed as the convective cloud fraction plus the larger of the stratiform and stratus cloud fractions.

The Rasch-Kristjánsson parameterization is a single moment bulk microphysics parameterization that prognoses cloud condensate (with liquid and ice as separate classes) and includes formulations of autoconversion, collection/ accretion, and sedimentation (Rasch and Kristjánsson, 1998; Neale et al., 2010). Autoconversion of liquid condensate begins when the condensate mixing ratio exceeds a threshold value; the threshold value varies solely as a function of pressure for liquid condensate and as a function of temperature for ice condensate. The autoconversion tendency is proportional to $q_l^{7/3}$ for in-cloud liquid condensate and to q_i^1 for in-cloud ice condensate. When cloud fraction is less than 100%, in-cloud condensate mixing ratios are estimated by dividing the cell-mean mixing ratio by cloud fraction (or by 2% if cloud fraction is less).

In anticipation of Section 6.6.2, in which we compare CAM4 and CAM5 simulations, we also summarize some relevant details of the CAM5 cloud and precipitation parameterizations, which are described fully by Neale et al. (2012). CAM5 uses the macrophysics parameterization described by Park et al. (In Preparation) and Neale et al. (2012) and the Morrison and Gettelman (2008) microphysics parameterization. In the Park macrophysics parameterization, stratiform coverage is exclusively a function of relative humidity when relative humidity goes above a specified threshold (the threshold algorithm is the same as in CAM4); the functional form comes from assuming that relative supersaturation has a triangular distribution within each cell (see Neale et al. (2012) for the exact form). The CAM5 physics package does not calculate a separate stratus cloud fraction, and total fraction is calculated as the sum of the stratiform and cumulus cloud fractions.

The Morrison-Gettelman scheme (Morrison and Gettelman, 2008; Gettelman et al., 2008; Neale et al., 2012) is a bulk two moment microphysics parameterization that prognoses cloud condensate (with liquid and ice as separate classes) and cloud droplet number. It includes formulations of droplet activation, condensation/deposition, evaporation/sublimation, autoconversion, accretion, collection, sedimentation, homogenous and heterogenous freezing, and ice melting. The autoconversion tendency is proportional to $q_l^{2.47} N^{-1.79}$ for in-cloud liquid condensate. Autoconversion of in-cloud ice condensate uses a formulation that converts part of the upper fraction of the assumed cloud number and ice mixing ratio distributions into snow at a characteristic 3-minute timescale. The liquid and ice autoconversion tendencies are both proportional to the liquid and ice cloud fractions respectively. When cloud fraction is less than 100%, in-cloud condensate mixing ratios are estimated by dividing the cell-mean mixing ratio by cloud fraction (or

Parameter Name	Value	Default	units
Deep convection precip. production efficiency	0.045	0.0035	unitless
Convective precipitation evaporation efficiency	$1.0 \cdot 10^{-6}$	$1.0 \cdot 10^{-6}$	unitless
Shallow convection precip production efficiency	$1.0 \cdot 10^{-5}$	$1.0 \cdot 10^{-4}$	unitless
Shallow convection CAPE removal timescale	1800	1800	s
Stratiform precipitation evaporation efficiency	$5.0 \cdot 10^{-6}$	$5.0 \cdot 10^{-6}$	unitless
Threshold for autoconversion of cold ice	$2.0 \cdot 10^{-5}$	$1.8 \cdot 10^{-5}$	kg/kg
Threshold for autoconversion of warm ice	$40.0 \cdot 10^{-5}$	$20.0 \cdot 10^{-5}$	kg/kg
Threshold for autoconversion of liquid droplets	$1.0 \cdot 10^{-6}$	$1.0 \cdot 10^{-6}$	m
Minimum RH threshold for high stable clouds	0.70	0.77	unitless
Minimum RH threshold for low stable clouds	0.91	0.92	unitless
Threshold for low stable cloud classification	75000	75000	Pa
Stokes ice sedimentation fall speed	1.0	1.0	m/s

Table 1: A list of tuning parameters and values used in this study in comparison to default values from a 1-degree simulation with the Finite Volume dynamical core.

by 0.01% if cloud fraction is less).

Throughout the manuscript, we refer to non-convective precipitation as stratiform precipitation (i.e., precipitation from the Rasch-Kristjánsson paramterization in CAM4 and from the Morrison-Gettelman parameterization in CAM5). We distinguish between resolved and unresolved stratiform precipitation as precipitation coming from columns with and without 'resolved clouds' respectively, which we define in the next section.

3 Scaling in CAM4

3.1 Scaling of Cloud Sizes

To compare the scaling behavior of CAM4 with the observations from Wilcox and Ramanathan (2001) and Wood and Field (2011), we follow the methodology of Wood and Field (2011) to identify contiguous clouds from instantaneous, 3-hourly model output. We define such contiguous clouds as 'resolved clouds' (i.e., clouds with a horizontal area at least as large as a model grid cell). Following Wood and Field (2011), we classify a resolved cloud in the model as a set of one or more contiguous grid columns where the column-total cloud fraction is greater than 99%. We define contiguous columns as those that share a side, and we utilize a recursive algorithm to identify contiguous sets of cloudy columns. As in Wood and Field (2011) and Yuan (2011), we find that our results are insensitive to whether or not we include corner-sharing cloudy columns as part of the same cloud. We also find that our results are insensitive to the cloud fraction threshold in the resolved cloud classification, with the exception that the global fractional coverage of resolved clouds approaches 100% as the cloud fraction threshold approaches 0% (which happens as a matter of course, since a threshold of 0% should identify every model cell as being cloudy). Clouds in nature are essentially proxies for saturated regions of the atmosphere, so the use of a high cloud fraction threshold allows for a simple comparison with observations, since it effectively identifies columns that contain a saturated or near-saturated region. This avoids the known difficulty of comparing the model cloud fraction field with observations (Bodas-Salcedo et al., 2011).

We derive the cloud size distribution $n(A_i)$ by adding up the number of clouds N_i with area between the logarithmically-spaced bin boundaries A_{i+} and A_{i-} Wood and Field (2011). We then normalize that count by the total area sampled A_{tot} and by the bin-spacing to obtain $n(A_i) = N_i/[A_{tot}(A_{i+} - A_{i-})]$. The resulting cloud area distributions are shown in Figure 1.

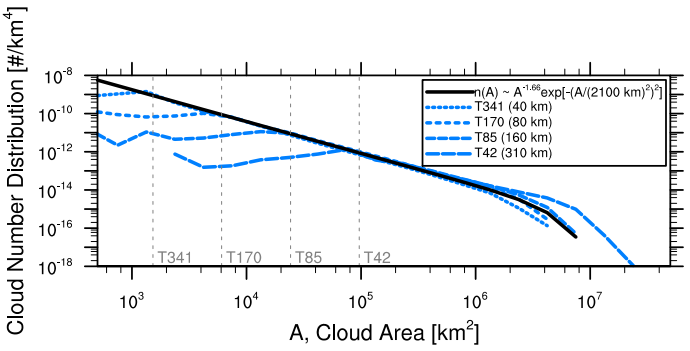

Figure 1: The cloud area distribution from Wood and Field (2011) (solid black curve) and from CAM4 aquaplanet simulations at four resolutions: T42, T85, T170, and T341. The solid black Wood-Field curve shows the distribution that would result if the cloud-length and cloud-area distributions have the same form.

Figure 1 shows that the modeled cloud area distributions closely follow a power-law distribution over a wide range of

cloud sizes. The CAM4 simulations produce a substantial number of clouds with areas that are smaller than the nominal resolution. In Figure 1, these clouds are identifiable by the segments of the number distributions where these distributions flatten and break from the power laws distributions that prevail at larger cloud sizes. These breaks occur approximately at the scale corresponding to the equatorial resolution of the model, so we include vertical lines in Figure 1 to denote the equatorial resolution of each simulation. These mostly single-cell clouds come from the high-latitude and polar regions where the meridians converge and the grid cells are relatively small and have a high aspect ratio. Since the fractional coverage of these clouds is small, representing approximately one percent of the total cloud area, we ignore them for the remainder of this discussion and focus only on clouds that are at least as large as an equatorial grid cell.

The modeled cloud area distributions closely follow a power law distribution from the scale of the simulation's nominal resolution up to a maximum cloud size that depends on model resolution. All the simulations exhibit a scale-break at large cloud sizes in a way that is consistent with the Wood-Field cloud-length distribution. We fit the function $N(A) = cA^{\beta}\exp[-(A/A_{brk})^2]$ to the area distribution from each simulation to determine the power law slope, β, and the location of the scale-break, A_{brk}. The power law slopes from the individual simulations vary systematically with resolution and range from -1.33 at T42 to -1.68 at T341. Table 2 presents estimates of the $N(A)$ parameters, with estimated errors, obtained by a least-squares fit (in log-log space) of $N(A)$ to the model output. Of all the simulations, only the T341 simulation has a value of β that falls within the range of observed slopes between -1.66 and -1.80 (Wood and Field, 2011). Wood and Field (2011) use a synthetic cloud dataset to show that the ratio of domain size to pixel size strongly reduces the magnitude of the measured power law slope when the ratio is less than approximately 1000:1. While their result applies to the effect of an instrument's spatial resolution, it is possible that this effect may also apply to the resolution of a model simulation. In the CAM4 simulations, these ratios are roughly 128:1, 256:1, 512:1, and 1024:1 for the T42, T85, T170, and T341 resolutions respectively. If this domain-to-cell-size rule holds for atmospheric models, then it would make sense that the T341 simulation is the only one with a power law slope that is within the range of the observed slopes.

The CAM4 cloud area distributions all exhibit a scale-break, though the location of this break also depends on model resolution. The breaks range from $9{\cdot}10^6$ km^2 at T42 resolution to $2.6{\cdot}10^6$ km^2 at T341 resolution (see Table 2). The systematic decrease in this scale-break reflects a monotonic downward trend in the number of massive cloud systems as resolution decreases in CAM. This is consistent with previous aquaplanet results using CAM that show that

	c	$\boldsymbol{\beta}$	$\mathbf{A_{brk}}$ **[km^2]**
T42	$(0.3 \pm 0.2){\cdot}10^{-5}$	-1.33 $\pm$ 0.05	$(9 \pm 1){\cdot}10^6$
T85	$(3.9 \pm 0.5){\cdot}10^{-5}$	-1.53 $\pm$ 0.01	$(4.5 \pm 0.2){\cdot}10^6$
T170	$(11 \pm 2){\cdot}10^{-5}$	-1.61 $\pm$ 0.01	$(3.1 \pm 0.4){\cdot}10^6$
T341	$(18 \pm 3){\cdot}10^{-5}$	-1.68 $\pm$ 0.02	$(2.6 \pm 0.6){\cdot}10^6$

Table 2: Best-fit estimate of the parameters in $N(A) = cA^{\beta}e^{-(A/A_{brk})^2}$ to the modeled cloud-area distributions from Figure 1.

global cloud fraction decreases systematically with increasing resolution (Williamson, 2008). By itself, Williamson's (2008) result indicates scale-incognizant behavior, since global cloud fraction should be constant with resolution if the subgrid cloud parameterizations are operating in a scale-aware way. Further, intuition suggests that as model resolution increases, the fraction of clouds that are resolvable should also increase. This can be expressed mathematically using the framework given in Wood and Field (2011). Wood and Field (2011) show that the mean cloud fractional coverage of clouds larger than area A, denoted by $f_c(A)$, is given by the first moment of the cloud size distribution, i.e. $f_c(A) = \int_A^{A_\oplus} A'n(A')\,dA'$, where the area of Earth $A_\oplus$ is used as the upper limit of integration. They also define the cumulative contribution of clouds, $C(A)$, as $f_c(A)$ divided by the total cloud fraction. $C(A)$ represents the relative fractional coverage of clouds greater than area A. If we replace the upper limit of integration $A_\oplus$ with ∞, which is an excellent approximation since the number distribution drops off rapidly for clouds larger than the scale-break A_{brk}, then $C(A)$ can be expressed as a ratio of two incomplete gamma functions:

$$\begin{aligned} C(A) &= \int_A^{\infty} An(A)\,dA \Big/ \int_0^{\infty} An(A)\,dA \\ &= \frac{\Gamma\left(\frac{\beta+2}{2}, \left(\frac{A}{A_{brk}}\right)^2\right)}{\Gamma\left(\frac{\beta+2}{2}, 0\right)} \end{aligned}$$

Figure 2 shows the relative fractional coverage of resolved clouds (Equation 1) as a function of horizontal scale (grid cell area) along with the estimated uncertainty derived from uncertainties in β and A_{brk} as described below. The black curve in Figure 2 is essentially the same curve as in Wood and Field (2011) (their Figure 6) except that we use $\beta = -1.73$, which is the mean of the -1.66 and -1.80 values from Wood and Field (2011). To examine the implications of uncertainty in the power law slope and location (or existence) of the scale-break discussed above, we also show a 1-σ estimate of the uncertainty in the relative coverage. We estimate this uncertainty by generating an ensemble of $C(A)$ curves using β and A_{brk} values within one

standard deviation of their mean. The spread in Figure 2 shows the minimum and maximum $C(A)$ values within this set. For the parameter uncertainty, we use $\sigma_\beta = 0.07$ and $\sigma_{A_{brk}} = 2 \cdot 10^6$ km^2. The uncertainty in β is estimated as half the difference between the slopes of the cloud chord distribution and the cloud area distribution presented in Wood and Field (2011), and the uncertainty in A_{brk} is estimated from the spread in scale-break parameters presented in Figure 3 of Wood and Field (2011)[2].

We interpret $C(A)$ as the fraction of total cloud cover that should be fully resolvable by a model with a nominal cell area of A. As expected, the relative contribution of resolvable clouds increases as theoretical model resolution increases in Figure 2. In other words, as model resolution increases, the partitioning of clouds should shift from the unresolved component to the resolved component. However, as noted above, CAM4 does not obey this behavior since as model resolution increases in CAM4, both the global cloud fraction and the relative contribution of resolved clouds systematically decrease. As noted in Wood and Field (2011), and as shown in Figure 2, even at the modest T85 resolution nearly 80% of global cloud cover should be associated with fully-resolved clouds. Instead only about 20% comes from resolved clouds. At T341 resolution, over 90% should come from resolved clouds, yet only about 10% actually does. Despite the excellent agreement on the slope of $n(A)$ between CAM4 and the Wood and Field (2011) data, this major difference in $f_c(A)$ occurs because CAM4 effectively has a smaller normalization coefficient on $n(A)$. The reason is that CAM4 has far fewer clouds than in observations even though the relative distribution of cloud sizes is in excellent agreement with observations.

Since cloud fraction in CAM4 is a diagnostic quantity that may exhibit its own resolution-dependent behavior, we have also performed this analysis using relative humidity itself to define 'cloudy' regions, and the analysis produces similar results (not shown). Specifically, the relative horizontal area of grid columns containing at least one grid cell with relative humidity above a given threshold (e.g., 99%) decreases systematically as resolution increases, similar to Figure 2. This occurs even though the size distribution of such areas follows a power law similar to Figure 1. This indicates that the scale-incognizant behavior shown in Figure 2 is not an artifact of how CAM4 defines cloud fraction, but rather it indicates that the model loses regions with high relative humidity as resolution increases.

Figure 2 points to two issues in CAM4. First, there are too few resolved clouds, and therefore global cloud fraction is improperly dominated by clouds that are implicitly smaller than a grid cell, i.e., cells with cloud fraction less than ∼100%. Second, the resolved fraction of clouds appears to converge to 0% as model resolution increases when instead it should converge to 100%. To show that the convergence toward zero is not an artifact of our analysis method, we replicate this analysis on a synthetic set of runs. We use data from the T341 simulation as the reference case, and we use nearest-neighbor interpolation[3] to obtain the corresponding T170, T85, and T42 versions of the same field; we use nearest-neighbor interpolation because it is the simplest interpolation method that preserves maxima and minima in the field, whereas conservative or bilinear interpolation methods would not (e.g., Accadia et al. (2003)). The resolved cloud fraction from the T341 simulation serves as an estimate of the total cloud fraction. Figure 2b shows the cumulative cloud distribution from this synthetic analysis. The curves essentially overlap, and as resolution increases, fractionally more clouds are resolved in a way that is consistent with our cloud number distribution analysis. Figure 2b explicitly demonstrates how a properly scale-aware model should behave.

3.2 Scaling of Precipitation Intensity

Following the method of Wilcox and Ramanathan (2001), we calculate the average precipitation rate over individual clouds and average the precipitation rate within a given cloud-size bin to obtain the average precipitation intensity as a function of cloud size. We show the dependence of precipitation rate as a function of cloud size for the four CAM4 aquaplanet experiments in Figure 3. We include the Wilcox and Ramanathan (2001) data (digitized from their Figure 5a) in Figure 3 for reference.

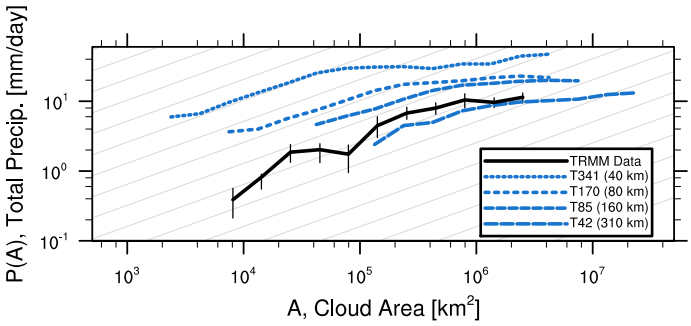

Figure 3: The cloud-area dependence of precipitation intensity from Wilcox and Ramanathan (2001) (solid black curve) and from CAM4 aquaplanet simulations at four resolutions: T42, T85, T170, and T341. The dashed grey lines show a power-law slope of 0.6, which is the best fit to the Wilcox and Ramanathan (2001) data.

In both the TRMM observations (Wilcox and Ramanathan,

[2]Specifically: $\sigma^2_{A_{brk}} = (2L_{brk}\sigma_{L_{brk}})^2 = (\,2 \cdot\ 2100\text{km} \cdot\ 500\text{km})^2$

[3]i.e., interpolation where the interpolation weights are 1 for the nearest point in the reference field and 0 for all other points. This effectively reduces to subsampling the T341 field every 2, 4, and 8 points for the T170, T85, and T42 grids respectively.

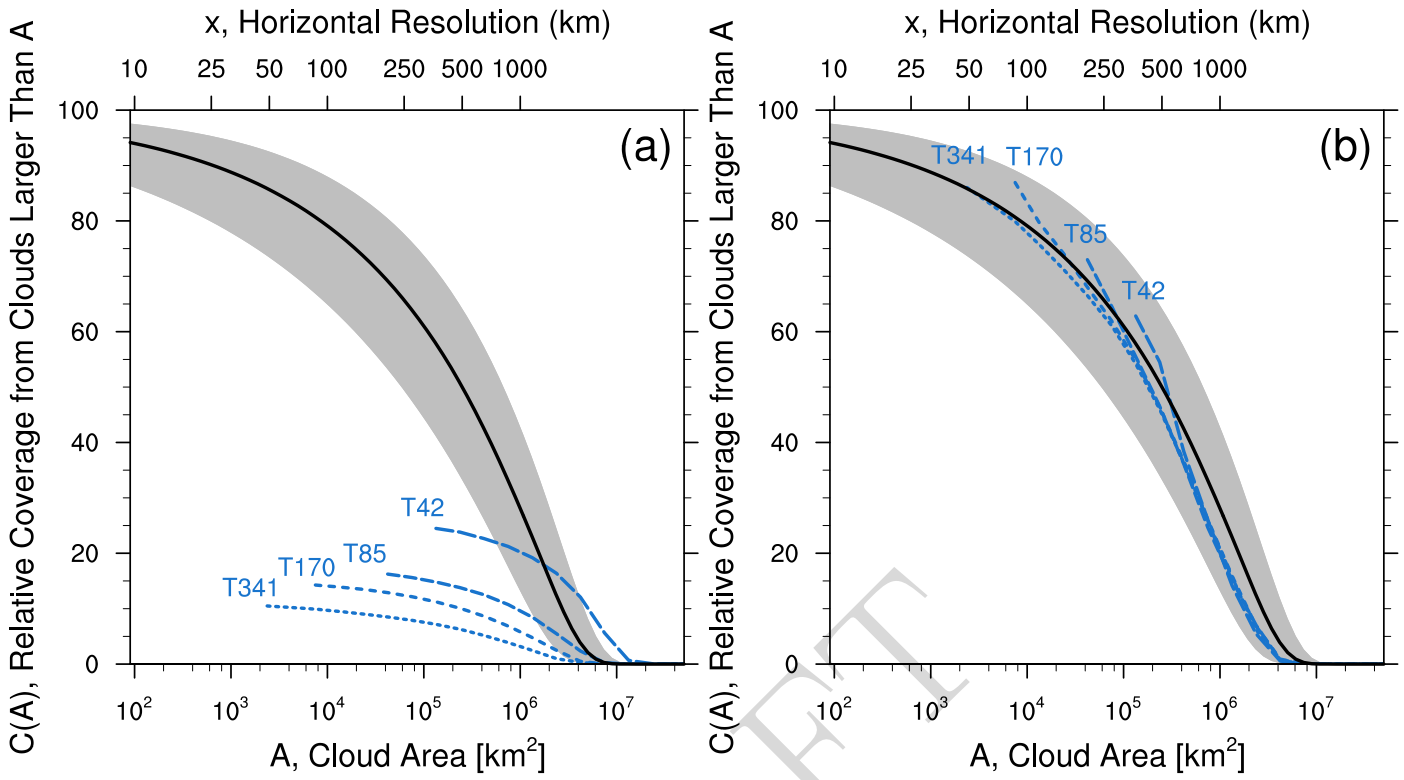

Figure 2: The relative fractional coverage of clouds that are larger than a given area as a function of that area, i.e., the percent of total cloud amount comprised of resolvable clouds. The black curve shows the contribution curve derived from a Wood-Field cloud area distribution ($n(A) \sim A^{\beta} \exp[-(A/A_{brk})^2]$). The grey swath shows the estimated uncertainty in the Wood-Field contribution curve given uncertainty in β and A_{brk}. The dashed grey lines show the resolution-dependence of the contribution of resolvable cloud fraction as derived from CAM4 aquaplanet simulations. (a) The resolution-dependence from actual simulations, and (b) the resolution-dependence from a synthetic set of simulation derived by interpolating the T341 simulation to the other resolutions. The curves in (b) are normalized by the same constant such that the T341 curve begins on the black line.

2001) and the CAM4 simulations, precipitation intensity increases as a nearly monotonic function of cloud size. While the relationship is not as clean as the cloud size distribution, it appears that precipitation intensity roughly follows a power law relationship with cloud size. A least-squares fit to the Wilcox and Ramanathan (2001) data yields a power law slope of $c = 0.59 \pm 0.04$, which we also show in Figure 3. It is notable that both the observations and the model output deviate substantially from the power law for large clouds. The precipitation rate ceases its steady increase when cloud sizes exceed a certain scale, though the scale at which the deviation occurs depends on model resolution. At present, we do not have an explanation for this leveling-off behavior, though we present evidence in Section 55.1 that it is a numerical artifact of the model dynamics.

4 Resolution-Dependence of the Resolved Fraction of Precipitation

Given a cloud size distribution and a precipitation rate that varies as a function of cloud size, the mean precipitation rate coming from clouds with areas between A_1 and A_2 can be defined as $\bar{P} = \int_{A_1}^{A_2} AP(A)n(A)\,dA$. While Wood and Field (2011) interpret this integral as the mean value of precipitation over all cloudy regions, the integral actually gives the precipitation averaged over all regions. This can be shown simply given that cloud fraction comes from the integral $f_c = \int An(A)\,dA$. If we assume that all clouds rain at a constant rate of $P(A) = P_0$, then the integral $\int AP(A)n(A)\,dA$ is equivalent to $P_0 \cdot \int An(A)\,dA = P_0 \cdot f_c$, which is the precipitation rate averaged over all areas. If the integral instead represented the cloudy-region average, as Wood and Field (2011) argue, then we should expect the

integral to return P_0 as the average. We emphasize this point here because it is critical in the following discussion.

The quantity of interest is the fraction of precipitation $F_R(A)$ coming from clouds that should be resolvable at a given model resolution represented by the area A of a model grid cell. This fraction can be written as the ratio of precipitation occurring in clouds larger than the grid-cell scale $\bar{P}(A > A_{res})$ to the total precipitation denoted by $\bar{P}(A < \infty)$. Following the discussion in Section 3, the cloud size distribution $n(A)$ and precipitation distribution $P(A)$ can be approximated by $n(A) = aA^{\beta} \exp -(\frac{A}{A_{brk}})^2$ and $P(A) = bA^c$ respectively, where A_{brk} is the area at which the scale-break in the cloud size distribution occurs. This ratio of integrals can be expressed as a ratio of incomplete gamma functions, which can be approximated by a Taylor expansion to yield a function that is a product of a power law and gaussian function of A:

$$
\begin{aligned}
F_R(A) &= \frac{\bar{P}(A' > A)}{\bar{P}(A' < A_{\infty})} \\
&= \frac{\int_{A}^{\infty} A' \cdot (bA'^{c}) \cdot (a \cdot A'^{\beta} e^{-(A'/A_{brk})^2})\, dA'}{\int_{0}^{\infty} A' \cdot (bA'^{c}) \cdot (a \cdot A'^{\beta} e^{-(A'/A_{brk})^2})\, dA'} \\
&= \frac{\Gamma\left(\frac{\beta+c+2}{2}, (\frac{A}{A_{brk}})^2\right)}{\Gamma\left(\frac{\beta+c+2}{2}, 0\right)} \\
&\approx 1 - e^{-(\frac{A}{A_{brk}})^2} \cdot \left(\frac{A}{A_{brk}}\right)^{\beta+c+2}
\end{aligned}
$$

The approximate form of the integral in Equation 1 gives some insight into how the resolved fraction equation behaves. The exponent given by $e = \beta + c + 2$, is greater than or equal to 0 since β is almost certainly greater than -2 (Wood and Field, 2011), and c appears to be positive according to Wilcox and Ramanathan (2001) and Figure 3. Adopting the best-fit value of $\beta \approx -5/3$ sets $e \gtrsim 2/3$, and we use $e \simeq 0.8$. This implies that the second term of Equation 1 is a monotonically increasing function of A/A_{brk} (assuming that the exponential term is approximately 1 for $A << A_{brk}$). As A decreases relative to A_{brk}, the second term in the equation approaches zero and so the resolved fraction approaches 1. Figure 1 and the cloud scaling data from Wood and Field (2011) indicate that $A_{brk} \sim 10^6 \mathrm{km}^2$, so one would expect a majority of precipitation to come from clouds that are larger than a model's grid scale ($A \sim 10^4 \mathrm{km}^2$) because $F_R \sim 1 - e^{-10^{-4}}(10^{-2})^{0.8} \sim 1$; Wilcox and Ramanathan (2001) come to a similar conclusion using satellite observations. While this result is sensitive to the scale at which the cloud distribution breaks, which Wood and Field (2011) show varies geographically, data from Wilcox and Ramanathan (2001) indicate that it is about $10^6 \mathrm{km}^2$ for the tropics. Median cloud size data from Wood and Field (2011) implies that it is instead about $(500\mathrm{km})^2 \sim 2.5 \cdot 10^5 \mathrm{km}^2$ in the tropics and approximately $10^{\,6}$ km^2 for the midlatitudes. Since most precipitation falls in these regimes (the tropics and the mid-latitudes), and the fraction of resolved precipitation at 100 km resolution should range from about 0.9 to 1 based on these scale-break values, nearly all global precipitation should come from clouds systems that are larger than a typical grid box. As Wilcox and Ramanathan (2001) aptly point out, this does not imply that a model should be able to resolve the physical processes that lead to precipitation, e.g. individual convective elements. It does imply, however, that most precipitation should come from grid columns where the cloud-area-fraction is 100%.

Figure 4 shows Equation 1, and the grey swath in Figure 4 shows the 1-σ uncertainty in this curve due to uncertainties in β, c, and A_{brk}. Following Section 3.3.1, this uncertainty is estimated by calculating $F_R(A)$ for combinations of c and A_{brk} within $\pm$1-σ of their mean values. We estimate the precipitation scaling parameter to be 0.59 $\pm$ 0.04 from a least squares fit to the Wilcox and Ramanathan (2001) data in Figure 3, however we use $c = 0.4$ and $\sigma_c = 0.2$ to evaluate F_R over a wider range of scaling parameters.

To demonstrate that the results discussed above do not result from approximating $P(A)$ as a power law, we include a digitized version the cumulative precipitation contribution presented in Figure 6b of Wilcox and Ramanathan (2001) (note that we in fact show one minus that curve). This curve falls within the error estimate of the integrated curve over most of its range. Therefore, we conclude that F_R is not particularly sensitive to the precise shape of $P(A)$.

As indicated by the analysis of the analytic approximation of the resolved fraction, and by Figure 4, F_R is close to 100% at the 100 km (10^4 km^2) scale of a typical global model. The lower range of the error estimate is greater than $F_R = 95\%$ at this scale. To re-emphasize the important point from above, this implies that nearly all precipitation in climate models should come from columns where the vertically-integrated cloud fraction is 100%.

The resolved fraction of precipitation in CAM4, shown by the end-points of the colored curves in Figure 4, is substantially lower than the resolved fraction implied by observations. The resolved fraction of precipitation ranges from about 50–60% in the four CAM4 simulations. Furthermore, the resolved fraction of precipitation decreases with increasing resolution. While the resolved fraction of precipitation in CAM4 does not seem to be converging toward 0% as with the resolved cloud coverage, it certainly is not converging toward 100% as observations (and intuition) imply it should.

Since the number distribution of clouds in CAM4 changes as a power law of cloud size (Figure 1), as does the precipitation intensity (Figure 3), Equation 1 implies that the

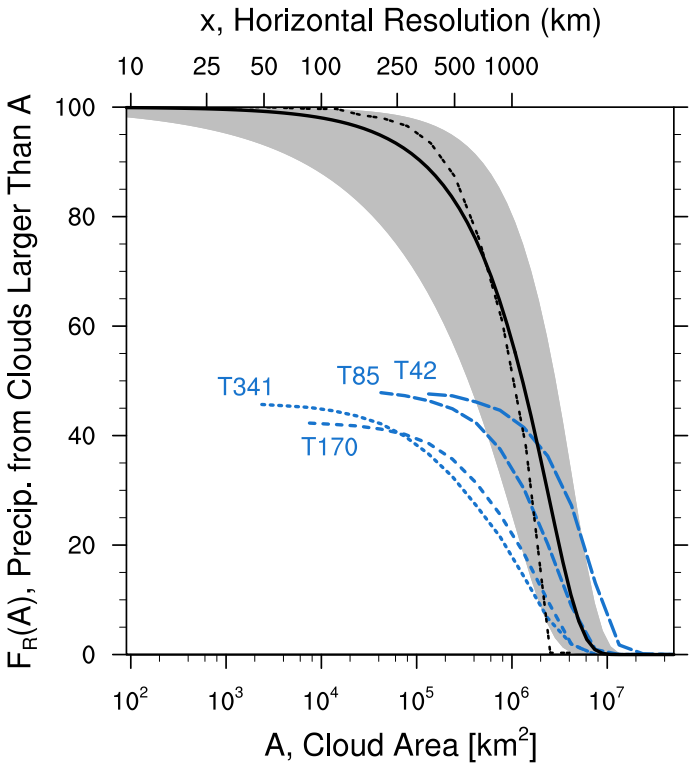

Figure 4: The resolution-dependence of the resolved fraction of stratiform precipitation coming from clouds that are larger than a given resolution. The dashed black curve shows the resolved fraction calculated directly using data from Wilcox and Ramanathan (2001), the solid black curve shows the estimated resolved fraction that results from assuming that the cloud area and precipitation-area distributions follow power laws, and the grey shading shows the 1-σ error in the estimated resolved fraction given errors in the power law distributions. The dashed grey lines show the actual resolution-dependence of resolved fraction from a set of idealized (aquaplanet) CAM4 simulations.

resolved fraction of precipitation in CAM4 should have a similar shape to the black curve in Figure 4. Indeed, the curve for each individual simulation in Figure 4 has a shape that is geometrically similar to the black curve. However, Equation 1 also implies that the CAM4 curves should basically overlap, such that as resolution increases, each new curve exposes more of the resolved-fraction vs horizontal-scale curve. This is clearly not the case.

5 Scale-Incognizance in Multiple Dycores

To verify that the resolution-dependent behavior presented in the previous sections is not an artifact of the specification of the model dynamics, we show that CAM4 exhibits this behavior for multiple dynamical cores (dycores). Additionally, we show that the Weather Research and Forecasting (WRF) model behaves similarly when used with the CAM4 parameterization suite, indicating that this problem likely originates in one or more of the CAM4 parameterizations.

The model simulations presented in this section were produced as part of a larger project[4] aimed at assessing the merits of various strategies for regional climate modeling, including limited area, and variable-resolution or high-resolution global modeling. We use output from the first stage of this project, in which these various strategies are compared in an idealized aquaplanet framework. Section 2 describes the experimental setup of these simulations. Physics parameters, including timestep, were held constant among all the simulations. The individual simulations are differentiated by the choice of model, dycore, horizontal resolution, and regional domain. The simulations include output from the tropical-channel WRF and CAM climate models. For the WRF model, only the Eulerian mass coordinate dycore is used, while the CAM simulations are based upon four different dycores including the Eulerian spectral transform dycore (Neale et al., 2010), the spectral element dycore (HOMME) (Dennis et al., 2012a), the finite volume (FV) dycore (Lin, 2004), and the Model for Prediction Across Scales atmospheric (MPAS-A) dycore (Rauscher et al., 2012). The WRF model has been modified to use the parameterizations of the CAM4 physics package, so that the dynamical core is the main difference between the CAM4 and WRF simulations presented here. The WRF simulations have been performed at two resolutions on a tropical band, with boundary conditions supplied by the T85 Eulerian dycore simulation: 25 km and 100 km. The global CAM simulations are performed using the Eulerian dycore at T85 and T341 resolutions, the FV dycore at 2-degree (220 km) and 0.5-degree (55 km) resolutions, the HOMME dycore at 220 km, 110 km, 55 km, and 28 km resolutions, and the MPAS-A dycore at 240 km, 120 km, 60 km, and 30 km resolutions. The MPAS-A dycore has also been used to produce a variable-mesh simulation with a 30 km resolution region centered in the tropics and 240 km resolution elsewhere. These various configurations of dycores and resolutions yield 15 different model simulations, which are listed in Figure 5.

The cloud-area algorithm in Section 33.1 utilizes the model-calculated total column cloud fraction in order to detect resolved clouds. Unfortunately, this total cloud variable was not among those saved in the instantaneous output archive from the 'Robust Regional Climate Modeling' CAM4 simulations, and the substantial computational cost of these simulations has prohibited re-running the simulations to archive this variable. Fortunately, a significant por-

[4]The Department of Energy Project 'Development of Frameworks for Robust Regional Climate Modeling'

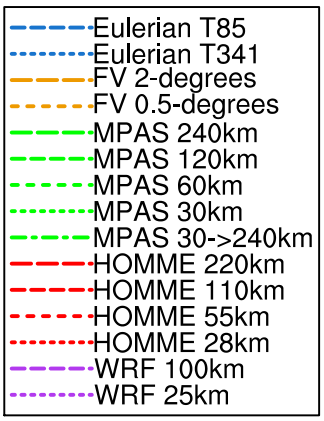

Figure 5: The legend for several figures in this manuscript; because of the size of this legend and the number of items, it is only presented once to conserve space.

tion of the cloud field in CAM4 is diagnosed solely from the relative humidity, which can be derived from the three-dimensional fields for temperature, pressure, and specific humidity included in the instantaneous output archive. We have directly implemented the necessary CAM4 parameterizations into our cloud-area code, including the procedures for calculating relative humidity, the dependence of stratiform cloud fraction on relative humidity, and the treatments of cloud geometrical overlap for the total-column cloud fraction. To be consistent with this definition of cloud, we also only use stratiform precipitation, whereas we had used total precipitation and total cloud fraction in Sections 33.1 and 33.2. As in Section 33.1, we define resolved clouds as any set of one or more contiguous cells with total stratiform cloud fraction greater than 99%. We performed the cloud-area analysis on the full last year of each 5-year model simulation. The T85 and T341 Eulerian dycore simulations described in Section 2 are identical to the T85 and T341 simulations described here, except that simulations in Section 2 were run for a shorter duration and saved a larger number of output variables (including, notably, total cloud fraction).

5.1 Precipitation Scaling

Figure 6a shows the cloud-size dependence of stratiform precipitation from all 15 simulations similar to the corresponding dependence of total precipitation depicted in Figure 3. In the Wilcox and Ramanathan (2001) data depicted in Figure 3, the precipitation intensity increases with increasing cloud size with a mean power-law slope of approximately 0.6 for clouds smaller than approximately $5 \cdot 10^4$ km^2 and is essentially invariant for clouds larger than this limit. Similar features are evident in the stratiform precipitation shown in Figure 6. With the exception of the MPAS-A dycore, precipitation in most of the dycores increases with a power law slope close to 0.6 for relatively small clouds, and all of the dycores exhibit some degree of slope-flattening for larger clouds. However, both the contrast between the high- and low-slope regions and the scale-break point, at which this flattening occurs differ appreciably across the various dycore and resolution combinations. The MPAS-A simulations exhibit almost no difference in slope between the high- and low-slope regions, whereas the slope actually reverses sign slightly in the low-slope region of the HOMME simulations.

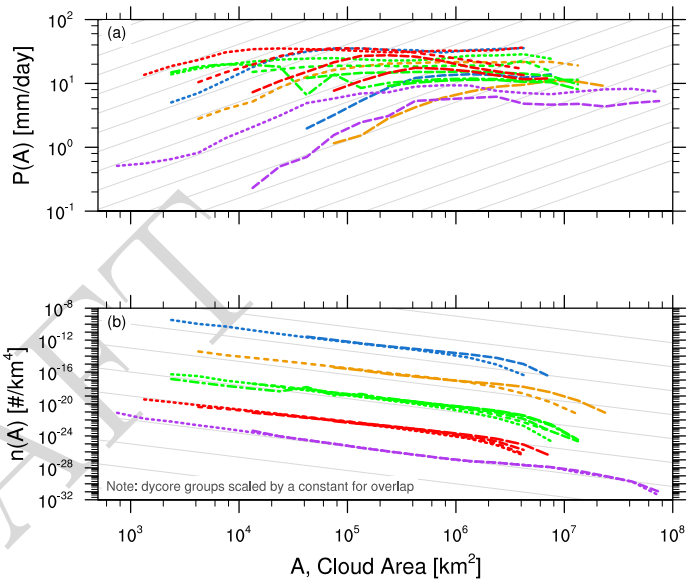

Figure 6: (a) Stratiform precipitation intensity as a function of cloud area for multiple dynamical cores and multiple resolutions in CAM4. The light grey lines depict a power-law slope of 0.6, which represents the best fit to the observations from Wilcox and Ramanathan (2001). (b) Cloud area distribution for multiple dynamical cores and multiple resolutions in CAM4. The light grey lines depict a power-law slope of $-5/3$, which represents the observations from Wood and Field (2011). Curves from a given dynamical core in (b) are scaled by a common arbitrary constant to provide vertical separation between the groups of curves. Table 5 shows the legend for both panels.

The scale-break point varies between 10^4 to 10^6 km^2 for the various combinations of resolutions and dycores. Despite this considerable dycore/resolution dependence, the different dycores do share a common feature, namely that the value of the scale-break increases with decreasing resolution. To determine the grid-cell size of clouds corresponding to the scale-breaks for each resolution and dycore, we perform a non-linear least-squares fit of two distinct scaling laws intersecting at a variable cloud amount where a

scale-break is introduced by construction. The value of this cloud amount that maximizes the variance explained by the two scaling laws gives an objective estimate of the area at which the scale-break occurs for each combination of resolution and dycore. We find that the scale-breaks are typically 4 ± 1 times the nominal resolution in terms of grid cell length. This implies that the curves from Figure 6 should collapse onto one another when horizontally normalized by the respective model resolutions. To demonstrate this, Figure 7 shows the same curves as Figure 6, but with the cloud size for each curve normalized by the area of an equatorial grid cell. Taking the square root of this value (cloud area divided by cell area) gives cloud sizes as measured by the characteristic grid-cell length of the cloud.

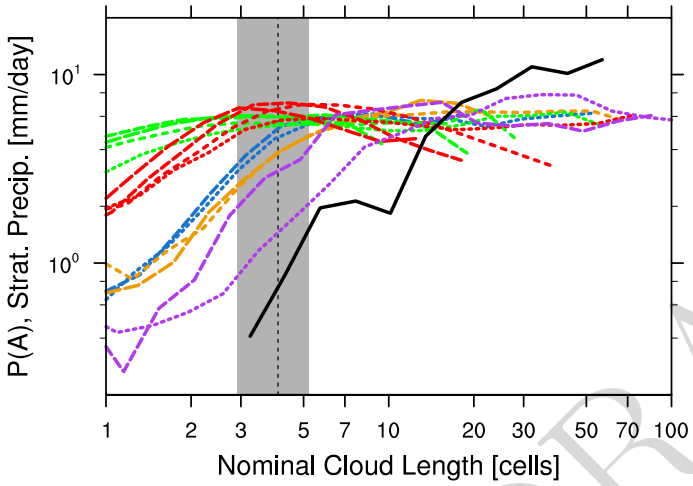

Figure 7: As in Figure 6a, but as a function of nominal grid-cell length instead of cloud area: i. e. the square root of cloud size divided by the area of an equatorial grid cell. The precipitation curves are multiplied by a constant so that they overlap in the flat portion of the curves. The vertical, dashed grey line shows the mean location of the scale-break point, as estimated by a least-squares fit to a line with two distinct slopes, and the vertical grey swath depicts the spread of these estimated break points. Table 5 shows the legend for the colored curves.

Figure 7 shows that for all of the dycores, precipitation rate increases sharply with a dycore-dependent slope from single-cell clouds up to clouds that are approximately four grid cells on a side. After this four-cell break, the precipitation rate is essentially independent of cloud size. The approximate slope (in log-precipitation versus log-cloud area space) is greater than -0.05 for most of the simulations, though it is approximately -0.2 for the simulations with MPAS-A at 240 km and 120 km and the simulations with HOMME at 220 km and 110 km.

The change in slope that occurs as cloud sizes approach a length of four grid cells might suggest that the relatively high slopes for areas smaller than the scale-break are caused by some numerical property or artifact of the underlying model dynamics. Since model dynamics, e.g., the numerical treatments of horizontal advection and diffusion, are consistent within a given dycore group, one might expect numerical artifacts of the dynamics to also be consistent within a given dycore group. This expectation is supported by the fact that the slopes are relatively consistent within dycore groups. For example, all of the MPAS-A simulations, which use high-order transport discretizations on a set of spherical centroidal Voronoi tessellations (Skamarock et al., 2012a), have slopes of relatively low magnitude for cloud areas smaller than the scale-break point. In contrast, the finite-volume simulations, which use second-order transport discretizations on a regular grid (Neale et al., 2010), have much larger slopes for clouds areas below the scale-break point. We hypothesize that the collective diffusive properties of the numerical schemes are responsible for this behavior, and if true this would imply that the slope of the curve should be sensitive to both explicit horizontal diffusion and implicit horizontal diffusion that results from the numerical formulation, e.g., use of monotone transport or upstream biased numerics.

5.2 Size Distribution and Resolved Fraction

Figure 6b shows the cloud size distribution for all 15 simulations. As in Figure 1, the cloud size distribution closely follows a $-5/3$ power law of cloud size over a wide range of cloud sizes up until a scale-break for clouds larger than approximately $2 \cdot 10^6$ km^2. For all the dycores, the number of extremely large clouds, i.e., clouds with areas larger than the scale-break, drops as resolution increases. Interestingly, all the uniform-resolution simulations from all the dycores have cloud size distributions that overlap almost perfectly, such that the higher-resolution simulations merely extend the power-law distributions to larger cloud areas. The maintenance of consistency with the scale-invariance of the cloud field at lower resolutions as small clouds are added with increasing resolution is precisely the sort of behavior that one should expect from a scale-aware mode.

Despite this excellent resolution-dependent behavior, all of the dycores exhibit the scale-incognizant change in the fraction of resolved clouds that is presented in Figure 2. Figure 8 shows how the fraction of cloud coverage that comes from resolved clouds changes as a function of resolution and dycore. As noted in Section 53.1, we expect that as resolution increases, the fraction of resolved clouds should also increase. Instead, within a given dycore group in Figure 8, the fraction of resolved clouds systematically decreases with increasing resolution. Since the curves in Figure 8 are essentially cumulative integrals of the curves in Figure 6b, this difference must be due to the system-

atic loss of extremely large clouds that occurs as resolution increases. The cloud number distribution drops systematically with increasing resolution in the rightmost portion of the curves in Figure 6b, and this is the only place where the curves within a given dycore group do not overlap. This loss of large clouds can be viewed as a resolution-dependent change in the location of the cloud number distribution scale-break. To demonstrate this objectively, we estimate A_{brk} from a least-squares fit of the Wood-Field $n(A)$ to the cloud size distributions from the uniform mesh CAM4 simulations. Figure 12 shows that A_{brk} decreases systematically with increasing resolution for each dycore.

Similarly, while the resolved fraction of stratiform precipitation (Figure 9) decreases systematically with increasing resolution, we have shown in Section 4 that it should systematically increase. Though Equation 1 is based on the analysis from Wilcox and Ramanathan (2001) for total precipitation, it can also be applied to stratiform precipitation in CAM4, since Figure 6a shows that stratiform precipitation scales roughly as a power law. Therefore Equation 1 also represents how the resolved fraction of stratiform precipitation in CAM4 should change with resolution, which is opposite of how it changes in Figure 9.

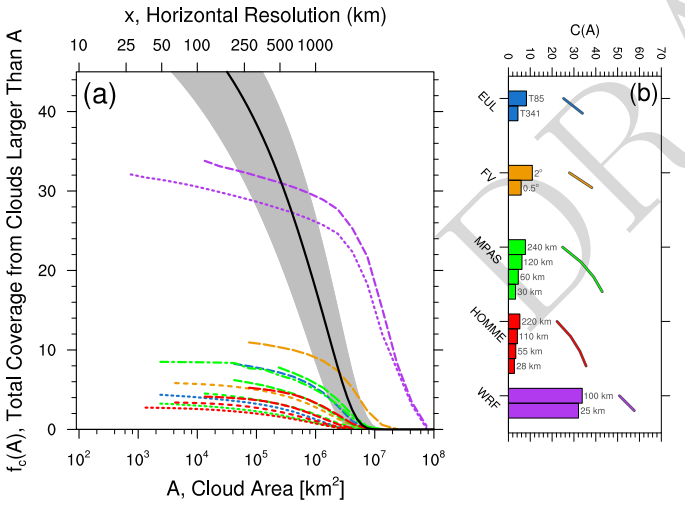

Figure 8: (a) $F_c(A)$, The fraction of area covered by clouds greater than area A for multiple dynamical cores at multiple resolutions. Note that the vertical scale is reduced to show details of the model curves. (b) The resolution-dependence of resolved cloud coverage for each dycore. The bars show the modeled resolved cloud coverage, and the adjacent curves show the resolution-dependence expected from Equation 1. See Section 5 for a discussion of the alternate definition of cloud used for these simulations. Table 5 shows the legend for the colored curves.

The curves in Figure 9 are effectively cumulative inte-

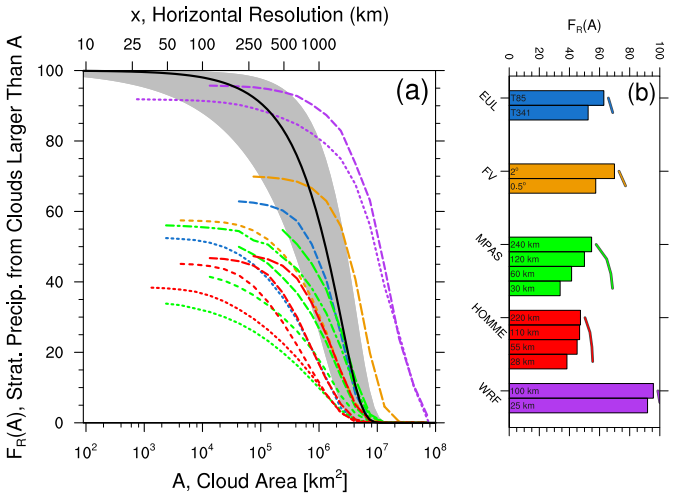

Figure 9: (a) As in Figure 4, but for multiple dynamical cores at multiple resolutions. (b) The resolution-dependence of the resolved fraction of precipitation for each dycore. The bars show the modeled resolved fraction, and the adjacent curves show the resolution-dependence expected from Equation 1. Table 5 shows the legend for the colored curves.

grals of the precipitation distributions from Figure 6a and the cloud size distribution from Figure 6b. Therefore this scale-incognizant behavior could come from decreases in either the number density of resolved clouds or the precipitation intensity in resolved clouds with increasing resolution. However, Figure 6a shows that the stratiform precipitation rate systematically increases with increasing resolution for all cloud sizes (see also Figure 10b in Section 66.1). For a fixed cloud size distribution and fixed total precipitation rate an increase in the intensity of resolved precipitation should cause an increase in the resolved fraction of precipitation. We can therefore rule out the systematic change in precipitation intensity as being the direct cause of the scale-incognizant decrease in resolved precipitation with increasing resolution. We must instead conclude that a change in the number distribution of clouds is the direct cause of the systematic decrease in the fraction of resolved precipitation. As we previously concluded in this section, the systematic loss of extremely large clouds with increasing resolution is the cause of the systematic decline in resolved cloud fraction. We conclude here that this systematic loss of extremely large clouds is also the direct cause of the systematic decline in resolved precipitation.

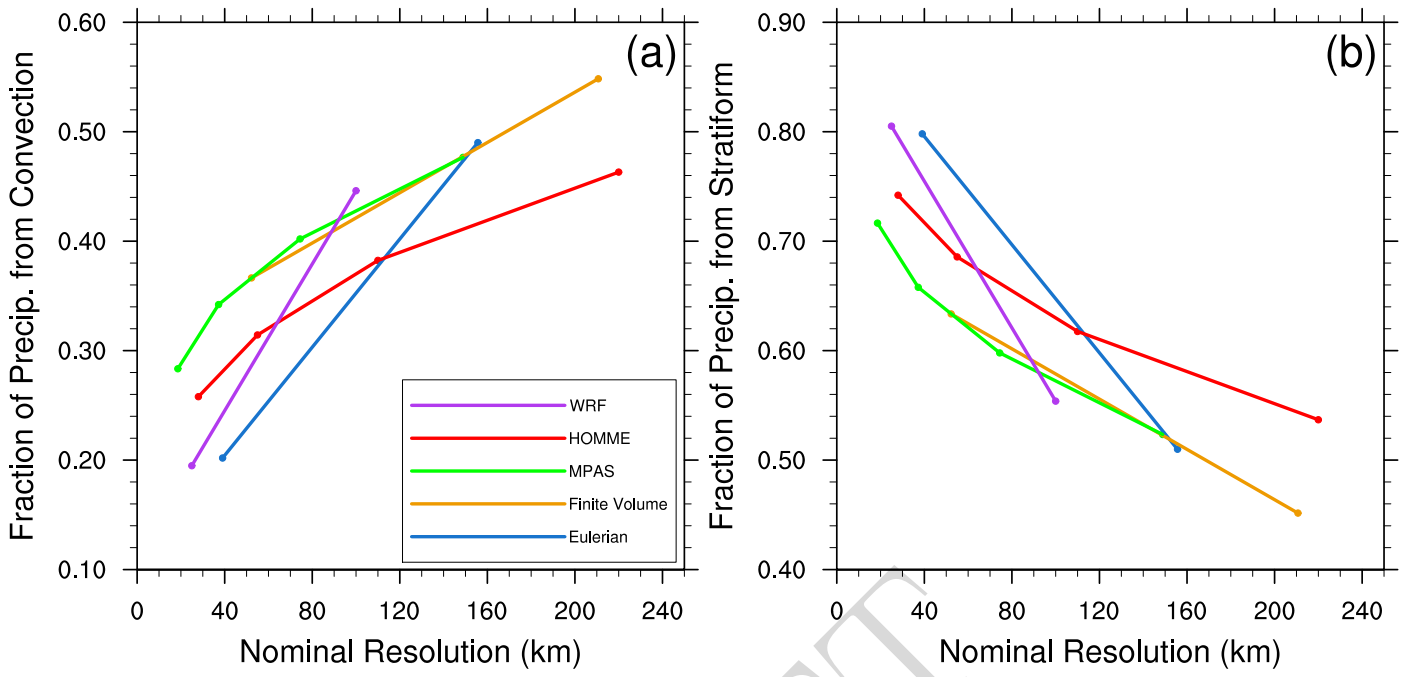

Figure 10: The fraction of precipitation coming from (a) convective precipitation, and (b) stratiform precipitation as a function of model resolution, for the various dynamical cores used in this study. The legend in (a) applies to both panels.

6 Scale-Incognizance of Multiple Parameterizations

6.1 Scale-Incognizance of Convection

What is the cause of this scale-incognizant behavior? While we do not have a definitive answer at this point, we can narrow the possible causes down to a likely few. The scale-incognizant results in Section 3 alone might lead one to speculate that some aspect of the model dynamics does not converge as resolution increases. However, Section 5 definitively shows that all of the dynamical cores exhibit this behavior. Given the dramatically different methods for solving the fluid equations that range from a spectral transform method on a regular grid in the Eulerian dycore to a finite volume method on Voronoi polygons in the MPAS-A dycore, it seems highly unlikely that the model dynamics are the root cause.

Li et al. (2011a) note that the non-convergent increase in precipitation extremes in CAM3 employing the Eulerian dycore appears to be related to an increase in the strength of vertical velocities. Their results suggest that model dynamics could drive the scale-incognizant behavior, but Williamson (2012) argues that the strong vertical velocities at high resolution in CAM4 are driven by latent heat release from the stratiform condensation parameterization. Since the latent heat release drives vertical motion and increases the vertical transport and horizontal convergence of moisture, this results in a positive feedback between the transport, latent heat release, and resulting buoyancy that in turn accelerates the vertical motion. Williamson (2012) shows that the excessive stratiform condensation results from an effective deactivation of the convective parameterizations that occurs when the model timestep is much smaller than the convective timescale. In the specific case evaluated by Williamson (2012), the model timestep of 5 minutes is an order of magnitude smaller than the 60-minute timescale for the deep convection. Williamson (2012) indicates that this effect is not as strong at lower resolutions and suggests that the coarser grid cannot support the strong horizontal convergence that results from this feedback. His results imply that the resolution-sensitivity of updraft strength and precipitation intensity is caused by the dampening of this condensation–updraft feedback as resolution decreases.

In the model runs presented here, the 10-minute timestep for the physics parameterizations is substantially less than the timescales of convection used in these runs of 30 and 60 minutes, respectively, for the shallow and deep convection. Following Williamson (2012), we should expect that convective precipitation is effectively deactivated at high resolution. Figure 10 shows that the fraction of precipitation generated by both of the convection schemes is relatively high and ranges from 40 to 50% for the lower resolution simulations, and it decreases into the range of 15–30% at higher resolutions at a rate that appears to be quite depen-

dent on the choice of dycore. Additionally, we find that updraft strength systematically increases with increasing resolution (not shown). This increase in updraft intensity, together with the relative decrease in convection, is consistent with Williamson's (2012) hypothesis. His work implies that a favorable convection-to-timestep ratio (i.e., of order 1 or larger) would allow an active set of convection parameterizations that might inhibit this feedback by removing atmospheric instability before the stratiform parameterization removes supersaturation by condensing water.

The resolution-dependence of the precipitation partitioning between the convective and stratiform components is consistent with results from Moncrieff and Klinker (1997) using the European Centre for Medium-Range Weather Forecasts model. They show that stratiform precipitation dominates over convective precipitation in T106 and T213 simulations of an organized convective cluster. They suggest that the problem is partly associated with the model underresolving the scale at which cumulonimbus clouds organize (∼20–200 km), which leads the resolved flow to organize into a super-cluster that drives stratiform precipitation at the cluster-scale (∼1000 km). They hypothesize that models with similar stratiform parameterizations (which CAM4 has) and resolution finer than T106 should exhibit similar behavior. This suggests that the resolution-dependent repartitioning of precipitation from convective to stratiform may be a model behavior that is not unique to CAM.

The resolution-dependence of convective precipitation shown in Figure 10 suggests scale-incognizance in the convection formulation. According to Williamson (2008), a common explanation for the resolution-dependence of convective precipitation and other measures of convective activity is that increasing resolution results in an augmentation of resolved convection and a reduction of parameterized convection. Williamson (2008) argues that this may be a weak premise. Given that the horizontal scale of convection is on the order of 10 km (Schumacher and Houze, 2003), convection should be occurring at the sub-grid scale in all of the simulations presented in this manuscript. Therefore, increasing resolution should not increase the amount of resolved convection in any of these simulations. A properly scale-aware convection formulation should produce a consistent fraction of the total precipitation, roughly 20% according to Schumacher and Houze (2003), for any climate simulation with a horizontal resolution larger than approximately 10 km.

6.2 Scale-Incognizance of Micro/Macrophysics

We show in Section 55.2 that the reduction in the resolved component of stratiform precipitation can be directly attributed to the loss of large, resolved clouds as resolution decreases. We hypothesize that either convective or stratiform processes are directly responsible for the loss of large clouds that leads to the scale-incognizant behavior. To test this hypothesis, we have performed a set of experiments in which we replicated the T42 and T85 simulations from Section 2, but with both convection parameterizations turned off in one set and sub-grid stratiform precipitation turned off in the other (specifically, autoconversion and sedimentation are restricted to originate from grid cells with at least 99% cloud fraction). We refer to the simulations as Convection-off and Subgrid-off respectively. To test whether the stratiform formulation itself causes the behavior, we have also run the T42 and T85 aquaplanet simulations with CAM5, which utilizes the Morrison-Gettelman microphysics and the Park macrophysics formulations instead of the Rasch-Kristjánsson and Zhang formulations of CAM4 (Neale et al., 2010, 2012). We refer to the combined micro- and macrophysics packages from CAM4 and CAM5 as the Rasch-Kristjánsson-Zhang (RKZ) and Morrison-Gettelman-Park (MGP) micro/macrophysics packages respectively. We perform the CAM5 simulations with a zonally and hemispherically symmetric prescribed aerosol dataset (including dust, sulfate, etc.), which is required by the CAM5 microphysics package.

Figure 11 shows the resolved cloud fraction and the resolved stratiform precipitation fraction from these experiments and from a control set of experiments (navy blue, dashed curves). Table 3 summarizes the results from these sensitivity tests. The Convection-off (yellow, dashed curves) and Subgrid-off (red, dashed curves) experiments show that neither of the convective parameterizations, which are both deactivated in Convection-off, nor sub-grid stratiform precipitation are solely responsible for the scale-incognizant behavior in CAM4. As in Figures 2, 4, 8, and 9, the resolved cloud fraction and the resolved stratiform precipitation fraction both decrease with increasing resolution in the Convection-off and Subgrid-off experiments. As in Sections 33.2 and 55.1, this scale-incognizant behavior in both experiments is caused by a loss of large clouds (not shown). The only component common to these three experiments is the RKZ micro/macrophysics package that controls the rates of condensation, evaporation, and precipitation formation in stratiform clouds. This strongly suggests that the RKZ package is the root cause of the scale-incognizant change in clouds and stratiform precipitation. If this is true, then a model configuration with a different set of micro/macrophysics parameterizations should have different resolution-dependent behavior. Figure 11 shows that CAM5, with the MGP micro/macrophysics package (green, dash-dotted curves), indeed exhibits scale-dependent behavior that is different from CAM4. Specifically, the resolved fraction of stratiform precipitation increases with increasing resolution in a scale-aware way, and the resolved cloud fraction increases from T85 to T170 resolution, though it decreases from T42 to T85.

It is difficult to conclude from Figure 11 and Table 3

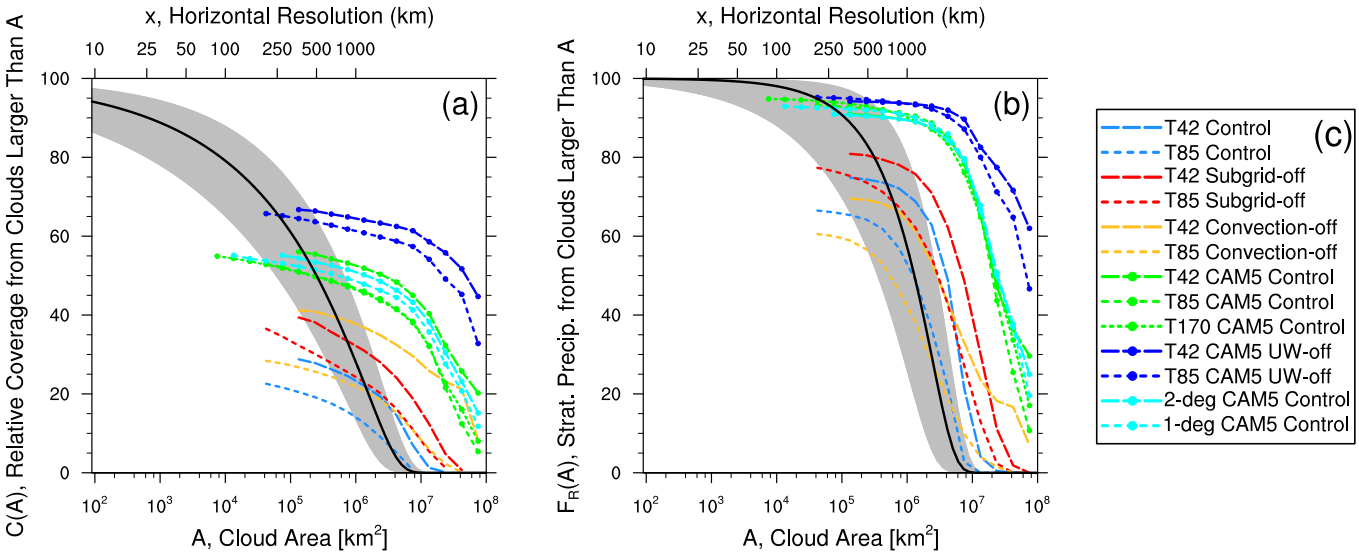

Figure 11: (a) The fractional coverage of resolved clouds, (b) the fraction of precipitation coming from convection as a function of model resolution from multiple sensitivity tests, and (c) the legend for curves in panels (a) and (b) The experiments using the CAM5 MGP micro/macrophysics parameterization are indicated by curves overlain with solid circles.

whether the CAM5 physics package yields a completely scale-aware model. The cumulative precipitation distributions overlap quite well among the three resolutions, and the cumulative resolved cloud fraction distributions overlap almost perfectly for the T85 and T170 simulations. However, the T42 distribution is systematically higher due to a higher proportion of massive clouds. Interestingly, the cloud number distributions for all the resolutions from the CAM5 APE simulations (not shown) have a power-law slope of approximately $-5/3$ for all cloud sizes. This is in contrast to the observations of Wood and Field (2011) and the CAM4 simulations, which exhibit a break in the distribution for clouds with a chord length longer than about 2000 km. That CAM5 has a systematically higher global and resolved cloud fractions of approximately 80% and 40%, respectively, relative to CAM4 may be due to the existence in CAM5 of semi-planetary-scale cloud systems that cover at least 10% of Earth's area.

To ensure that the more scale-aware features of the CAM5 simulations are due to the MGP micro/macrophysics package, and not the different boundary layer and shallow convection parameterizations, we have also run T42 and T85 CAM5 simulations with the CAM4 versions of these parameterizations (blue, dash-dotted curves). In these 'CAM5 UW-off' experiments, the new UW parameterization is replaced with the Holtslag-Boville parameterization for the boundary layer and the Hack parameterization for shallow convection. Figure 11 and Table 3 shows that the results are similar to the basic CAM5 simulation. Specifically, the resolved stratiform fraction curves change in a scale-aware way, the resolved cloud fraction drops between the T42 and T85 simulations, and semi-planetary-scale clouds exist. Further, a test with the FV dycore (cyan, dash-dotted curves) shows a change in resolved cloud fraction between the 2-degree and 1-degree simulations, indicating that this resolution-dependence is not solely due to an interaction between the Eulerian dycore and the CAM5 physics. These tests show that the MGP micro/macrophysics pacakge is responsible for changing the resolution-dependence of clouds and precipitation in the CAM5 simulations, which is further evidence that the RKZ micro/macrophysics package is the origin of the scale-incognizant changes in clouds and stratiform precipitation in CAM4. Because the microphysics and macrophysics parameterizations are closely coupled in both CAM4 and CAM5, it is difficult to devise a simple experiment that isolates one from the other to further narrow down whether the microphysics, macrophysics, or both parameterizations drive the scale-incognizant behavior.

Experiment	$\Delta F_c/\Delta Res.$	$\Delta F_R/\Delta Res.$
CAM4 Control	+	+
CAM4 Subgrid-off	+	+
CAM4 Convection-off	+	+
CAM5 Eulerian	+ & -	-
CAM5 FV	+ & -	-
CAM5 UW-off	+ & -	-

Table 3: A table summarizing the main results from the sensitivity tests shown in Figure 11. The $\Delta F_c/\Delta Res.$ and $\Delta F_R/\Delta Res.$ columns show the sign of the slope of the resolved fraction of cloud cover and precipitation respectively. The cells with '+&-' indicate ambiguous results. We define the Δ operator as the high resolution quantity minus the low resolution quantity. For both F_c and F_R, these slopes should be negative for a scale-aware model.

7 Discussion

Constraints on the various components of precipitation offer a framework in which to understand proper scale-aware behavior. Total precipitation is dynamically constrained to be insensitive to resolution, since global radiative-convective equilibrium requires this to be approximately 3 mm·day^{-1} to balance the radiative flux divergence across the troposphere. As argued above, convective precipitation should always be a sub-grid scale phenomenon in climate models with resolutions greater than about 10 km, and so convective precipitation should be insensitive to resolution in such models. If we view total precipitation as the sum of convective and stratiform components (i.e., $P_T = P_C + P_S$), then this implies that total stratiform precipitation should also be insensitive to resolution, though the partitioning between its unresolved and resolved components should change with resolution. We show in Section 4 that this partitioning should change as $F_R \sim 1 - x^\alpha$, where x is the grid area and α is a scaling parameter related to the scaling parameters from the cloud number distribution and from the cloud-size dependence of precipitation intensity. Furthermore, Figure 4 shows that at least 90% of the stratiform precipitation should occur in cloud systems larger than 250 km, and therefore the unresolved component of stratiform precipitation should be small and only weakly dependent on resolution in modern climate models with resolutions finer than 250 km.

In a model with a scale-aware set of precipitation parameterizations, global averages of the precipitation components should behave in the following way: convective precipitation should be constant with resolution, total stratiform precipitation should be constant with resolution, and the portion of precipitation coming from partially-cloudy grid columns should be small and should decrease as resolution increases. In contrast to this behavior, convective precipitation in CAM4 decreases by 15–30% as resolution increases (Figure 10a), stratiform precipitation increases by 15–30% (Figures 3 and 10b), the portion of precipitation coming from partially-cloudy grid columns is large (30–70%), and this unresolved component increases by approximately 20% as resolution increases (Figure 4). In other words, as resolution increases in CAM4, precipitation increasingly becomes inappropriately dominated by sub-grid scale stratiform "storms". We show evidence in Section 6 that the convective parameterization likely causes the scale-incognizant repartitioning of precipitation between the stratiform and convective components, and the micro/macrophysics package causes the scale-incognizant reduction in resolved cloud coverage and resolved precipitation. The MGP micro/macrophysics parameterizations in the CAM5 physics package appears to improve the scale-incognizant cloud and stratiform-precipitation behavior, but the scale-incognizant resolution-dependence of the relative contribution of convection remains.

The scale-incognizant behavior of the RKZ package likely explains results from a number of recent studies showing strong decreases in total cloud coverage and intensification of stratiform precipitation in CAM4 as resolution increases (Williamson, 2008; Levy et al., In Review; Rauscher et al., 2012). We do not yet have an explanation for why the RKZ package seems to drive such strong resolution-dependent behavior, but a future study that explains this behavior would be invaluable. An understanding of the causes of scale-incognizance could help ensure that future model development efforts produce scale-aware model components.

As we note in Section 5.5.2, the scale-incognizant decrease of resolved, stratiform precipitation can be attributed to a loss of large clouds as resolution increases, and this loss of large clouds is equivalent to the scale-break in the cloud size distribution shifting toward smaller scales. Therefore, understanding why the scale-break in the cloud-size distribution shifts toward smaller clouds as resolution increases is key to understanding the scale-incognizant behavior of precipitation in CAM4. Wood and Field (2011) hypothesize that the Rossby radius of deformation may set the size at which this scale-break occurs. If this is true, then it is plausible that resolution-dependence of the Rossby radius of deformation may explain the resolution-dependence of the scale-break. In Figure 12, the size of each point is proportional to the mean Rossby radius of deformation for that simulation. We approximate the Rossby radius as $R = |f|^{-1} \cdot \sum_{k=15}^{26} N_k \cdot \Delta z_k$, where f is the Coriolis parameter, k is the model level (ranging from approximately 250 hPa to 1000 hPa, which we chose to roughly span the troposphere), N_k is the Brunt-Väisälä frequency, and Δz_k is the layer thickness (Chelton et al., 1998). We calculate the mean Rossby radius as the mean in time and space (for latitudes greater than 5^o) weighted by the Coriolis parame-

ter to avoid biasing the estimate toward Equatorial values. Figure 12 indicates that the Rossby radius does not vary systematically with resolution, while the scale-break tends to decrease with increasing resolution. If the Rossby radius sets the scale at which the cloud size distribution breaks from a power law, then we should expect that the Rossby radius would also decrease with increasing resolution. That it does not indicates that the Rossby radius of deformation does not set the scale-break in these CAM4 simulations. While this provides evidence that the Rossby radius is not the sole quantity that determines the scale-break, it does not indicate whether the Rossby radius has any influence on the scale-break. Additional model experiments (e.g., sensitivity studies with the Coriolis parameter) will be necessary to investigate such a connection. Further work will be necessary to understand the scale-incognizant loss of large clouds, and the resulting loss of resolved precipitation, as resolution increases in CAM4 simulations.

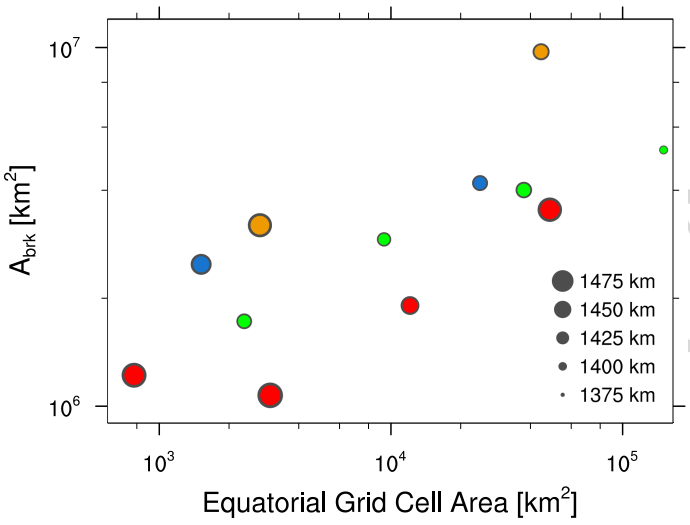

Figure 12: The scale at which the cloud number distributions from the CAM4 simulations depart from a power law as a function of model resolution. The color of the points indicates the dynamical core (blue ⇒ Eulerian, orange ⇒ FV, green ⇒ MPAS-A, red ⇒ HOMME), and the size of each point is proportional to the mean Rossby radius of deformation for that simulation.

In the two manuscripts describing variable-mesh capabilities in CAM, only CAM4 physics has been used (Levy et al., In Review; Rauscher et al., 2012). Currently, the MPAS dycore only works with CAM4 physics, although a new, non-hydrostatic version with CAM5 physics is currently in development (Skamarock et al., 2012b), and the SE dycore has not been extensively tested with the CAM5 physics. The apparent improvements in the scale-aware behavior of the CAM5 physics package, combined with the fact that it is now the core atmospheric model for the Community Earth System Model package, make it the logical alternative to CAM4 for variable-mesh modeling. However, CAM5 still requires some additional work to become a fully scale-aware model.

Our brief tests with CAM5 in aquaplanet mode indicate the following deficiencies with respect to scale-awareness: (1) there is a distinct jump in the resolved cloud fraction from T42 to T85 resolution (and from 2-degree to 1-degree with the FV dycore); (2) the fraction of precipitation coming from convection changes strongly with resolution as in CAM4; and (3) CAM5 does not exhibit the scale-break in the cloud number distribution that is present in CAM4 and that has been observed by Wood and Field (2011) (i.e., there are a significant number of planetary-scale cloud systems). Issue (1) indicates that there is some form of implicit resolution-dependence in the MGP micro/macrophysics parameterization. It is possible that a detailed investigation into the factors causing the implicit resolution-dependence of the RKZ micro/macrophysics package may reveal similar factors in the MGP micro/macrophysics parameterization. Issue (2) is not surprising, since both CAM4 and CAM5 utilize the Zhang et al. (2003) deep convection parameterization. Efforts like those described by Park (2012) may improve the scale-aware behavior of the convection parameterization. It is not immediately clear what causes issue (3), though it is possible that this is an artifact of using our cloud-clustering algorithm on a field in which a majority of the cells have resolved clouds. Since the cloud field is effectively more crowded, more clouds may combine to make mega-clusters. An alternative algorithm that discriminates clouds based on physical properties (e.g., cloud top temperature or vertical connectedness) may not behave in such a way. This could be tested either by using this algorithm on a synthetic cloud field with high cloud fraction, or by tuning CAM5 to have a lower cloud fraction. If it can be shown that issue (3) is not an artifact of the clustering algorithm, then a detailed comparison between the two CAM microphysics parameterizations may yield insight into why the MGP package produces a cloud field with planetary-scale clouds and the RKZ package does not.

This study has two important limitations: it treats the entire atmosphere as a single layer, and it does not consider the impact of vertical resolution. Pressel and Collins (2012) show that the scaling of water vapor differs distinctly between the boundary-layer and the free-troposphere. This suggests that an analysis of cloud scaling at different levels of the atmosphere may yield cloud size distributions with different slopes at different levels, which would affect the shape of the resolved cloud fraction ($C(A)$) and resolved precipitation fraction ($F_R(A)$) curves. If the power-law slope of the cloud size distribution depends on height in the atmosphere, then changing vertical resolution might change the power-law slope calculated by treating the atmosphere as a

single layer as we do in this analysis. Adding vertical layers to a specific section of the atmosphere might cause more clouds to be resolved in that section, which would weight the 'net-tropospheric' cloud size distribution toward that of the tropospheric section with additional layers. Analysis of vertically-resolved cloud observations, such as those from CloudSat (Stephens et al., 2008), could provide a height-resolved constraint on cloud scaling.

We argue that in the paradigm of variable-mesh models, a primary goal of model development should be to ensure that fields that are known to have scale-invariant statistics maintain that scale-invariance across resolution transition zones. This is not the case in variable-resolution simulations using CAM4 physics (Levy et al., In Review; Rauscher et al., 2012). Further, a primary goal of model tuning in this paradigm should be to ensure that the integrals of such scale-invariant quantities match with observations. In the case of clouds, this means that model development efforts should aim to produce a cloud number distribution that maintains a $-5/3$ power-law slope across the mesh transition regions, and model tuning efforts should aim to produce a cloud field in which resolved clouds cover approximately two-thirds of the area of the globe. If modeled cloud systems can be made to exhibit the scaling of optical properties observed in real clouds (Wood and Field, 2011), then perhaps global radiative balance will naturally follow as long as the cloud field is properly tuned. Conversely, variable mesh models that obey proper cloud size scaling behavior, but not cloud optical scaling behavior, might have high resolution regions with a radiative imbalance. Such regions would require anomalous horizontal convergence or divergence of energy to achieve energetic equilibrium.

8 Conclusions

This systematic study of the Community Atmosphere Model physics package in an aquaplanet framework has identified several distinctly scale-incognizant behaviors of CAM4. As resolution increases in CAM4 simulations, the model output changes in the following scale-incognizant ways: the precipitation budget becomes increasingly dominated by stratiform precipitation, more stratiform precipitation falls from unresolved clouds, the model resolves fewer large cloud systems, and the partitioning between resolved and unresolved clouds shifts toward unresolved clouds. Sensitivity tests implicate the deep convection parameterization as the source of the scale-incognizant increase in total stratiform precipitation and the microphysics parameterization as the source of the scale-incognizant changes in resolved cloud coverage and resolved stratiform precipitation. Tests with the CAM5 physics package show some improvements in scale-awareness, though we note some aspects that require further development: particularly the resolution-dependent repartitioning of convective and stratiform precipitation, which apparently originates in the deep convection parameterization.

Though this study demonstrates that the CAM4 microphysics parameterization and the CAM4/5 deep convection parameterization both lead to scale-incognizant behaviors, we do not have a good explanation for this behavior. A future study that investigates the physical reasons for these scale-incognizant behaviors may provide valuable information for the emerging field of scale-aware parameterization development. At very least, such a study would outline possible pitfalls in the design of scale-aware parameterizations.

The results from this study also show some interesting, but unexplained phenomena in CAM. In Section 5, we show that the cloud-area dependence of precipitation flattens for cloud clusters that are larger than about four grid cells on a side. This flattening, which occurs to some degree in all dycores at a grid-dependent scale, rather than a physical scale, suggests that the feature is numerical in origin. We speculate that it is somehow related to horizontal diffusion, but a detailed analysis of this phenomena may yield some insight into the numerical nature of CAM. Further, we show in Sections 33.1 and 5 that the CAM4 has a cloud number distribution with a scale-break, and that the location of this scale-break depends on the resolution. We demonstrate in Section 5 that the scale-incognizant behavior of resolved clouds and stratiform precipitation is directly related to the loss of extremely large clouds, which is expressed as a resolution-dependence of the location of this scale-break. Therefore, an investigation into the origin of the resolution-dependence of this scale-break should yield insight into why the CAM4 microphysics parameterization ultimately drives this scale-dependence. Additionally, such an investigation may provide some insight into what might control the location of this scale-break in the real world. Interestingly, CAM5 does not appear to exhibit this scale-break, though it is not clear whether this is due to an artifact of the cloud clustering algorithm, or whether it is an intrinsic quirk of the CAM5 microphysics parameterization; this issue should also be explored in a future study.

Scale-invariant and scale-dependent quantities are a natural touchstone for the development of variable-mesh models and particularly of scale-aware parameterizations within these models. In this study, we use the scale-invariance of the cloud number distribution to describe how cloud coverage should change with resolution. We combine this with the scale-dependence of precipitation to show how resolved precipitation should change with resolution. Numerous studies demonstrate the scale-invariance of various other atmospheric quantities, including momentum (Nastrom and Gage, 1985), temperature (Kahn et al., 2011), humidity (Kahn et al., 2011; Pressel and Collins, 2012), cloud water (Davis et al., 1996), and other variables. We expect that the results from such studies can be used to constrain or even develop scale-aware parameterizations. For example,

if scale-invariance can be demonstrated for the product of temperature or humidity with the wind components, then a description of the resolution-dependence of horizontal eddy fluxes would naturally follow. This information could then be used to develop an explicitly resolution-dependent horizontal eddy flux (diffusion) parameterization. Future scale-aware parameterization development efforts should make strong use of observations of scale invariance and scale dependence.

Acknowledgments.

The bulk of the conclusions from this analysis are based on a massive set of model output generated by the set of controlled experiments described in Section 5 using multiple dynamical cores and multiple resolutions in an aquaplanet framework. The authors of this study sincerely hope that others may make use of this dataset. These data are publicly available at the following link: http://portal.nersc.gov/cgi-bin/get_tape?/home/f/fli/www/CLIMES/Project_regional.

The authors would like to formally thank the following people for help with this manuscript: two anonymous reviewers whose thorough and insightful comments greatly improved the manuscript's clarity, Dr. Brian Medeiros of NCAR for advice on running CAM5 in aquaplanet mode, Dr. Peter Caldwell of LLNL for advice in implementing the Subgrid-off experiment, and Drs. Matus Martini of PNNL and Andrew Jones of LBNL for a meticulous proofreading of this manuscript. This research was supported by the Director, Office of Science, Office of Biological and Environmental Research of the U.S. Department of Energy Regional and Global Climate Modeling Program (RGCM) and used resources of the National Energy Research Scientific Computing Center (NERSC), also supported by the Office of Science of the U.S. Department of Energy under Contract No. DE-AC02-05CH11231.

References

Accadia, C., S. Mariani, M. Casaioli, A. Lavagnini, and A. Speranza, 2003: Sensitivity of precipitation forecast skill scores to bilinear interpolation and a simple nearest-neighbor average method on high-resolution verification grids. *Wea. Forecasting*, **18 (5)**, 918–932, doi:10.1175/1520-0434(2003)018⟨0918:SOPFSS⟩2.0.CO;2, URL `http://dx.doi.org/10.1175/1520-0434(2003)018<0918:SOPFSS>2.0.CO;2`.

Bodas-Salcedo, A., et al., 2011: COSP: Satellite simulation software for model assessment. *Bull. Amer. Meteor. Soc.*, **92 (8)**, 1023–1043, URL `http://dx.doi.org/10.1175/2011BAMS2856.1`.

Caldwell, P., H.-N. Chin, D. Bader, and G. Bala, 2009: Evaluation of a WRF dynamical downscaling simulation over california. *Climatic Change*, **95**, 499–521, doi:10.1007/s10584-009-9583-5, 10.1007/s10584-009-9583-5.

Chelton, D. B., R. A. deSzoeke, M. G. Schlax, K. El Naggar, and N. Siwertz, 1998: Geographical variability of the first baroclinic rossby radius of deformation. *J. Phys. Oceanogr.*, **28 (3)**, 433–460, URL `http://dx.doi.org/10.1175/1520-0485(1998)028<0433:GVOTFB>2.0.CO;2`.

Davis, A., A. Marshak, W. Wiscombe, and R. Cahalan, 1996: Scale invariance of liquid water distributions in marine stratocumulus. Part I: Spectral properties and stationarity issues. *J. Atmos. Sci.*, **53 (11)**, 1538–1558, URL `http://dx.doi.org/10.1175/1520-0469(1996)053<1538:SIOLWD>2.0.CO;2`.

Dennis, J., et al., 2012a: CAM-SE: A scalable spectral element dynamical core for the Community Atmosphere Model. *Int. J. of High Performance Computing Applications*, **26 (1)**, 74–89.

Dennis, J. M., M. Vertenstein, P. H. Worley, A. A. Mirin, A. P. Craig, R. Jacob, and S. Mickelson, 2012b: Computational performance of ultra-high-resolution capability in the Community Earth System Model. *International Journal of High Performance Computing Applications*,

26 (1), 5–16, doi:10.1177/1094342012436965, http://hpc.sagepub.com/content/26/1/5.full.pdf+html.

Gettelman, A., H. Morrison, and S. J. Ghan, 2008: A new two-moment bulk stratiform cloud microphysics scheme in the community atmosphere model, version 3 (cam3). part ii: Single-column and global results. *J. Climate*, **21 (15)**, 3660–3679, URL http://dx.doi.org/10.1175/2008JCLI2116.1.

Hack, J., J. Caron, G. Danabasoglu, K. Oleson, C. Bitz, and J. Truesdale, 2006: CCSM-CAM3 climate simulation sensitivity to changes in horizontal resolution. *J. Climate*, **19 (11)**, 2267–2289.

Kahn, B., et al., 2011: Temperature and water vapor variance scaling in global models: Comparisons to satellite and aircraft data. *J. Atmos. Sci.*, **68**, 2156–2168.

Kanamitsu, M. and H. Kanamaru, 2007: Fifty-seven-year california reanalysis downscaling at 10 km (CaRD10). Part I: System detail and validation with observations. *J. Climate*, **20 (22)**, 5553–5571, doi:10.1175/2007JCLI1482.1.

Kummerow, C., W. Barnes, T. Kozu, J. Shiue, and J. Simpson, 1998: The tropical rainfall measuring mission (TRMM) sensor package. *J. Atmos. Ocean. Tech.*, **15 (3)**, 809–817, doi:10.1175/1520-0426(1998)015%3C0809:TTRMMT%3E2.0.CO;2, URL http://dx.doi.org/10.1175/1520-0426(1998)015%3C0809:TTRMMT%3E2.0.CO;2.

Levy, M. N., J. R. Overfelt, and M. A. Taylor, In Review: A variable resolution spectral element dynamical core in the community atmosphere model. *Mon. Wea. Rev.*

Li, F., W. Collins, M. Wehner, D. Williamson, and J. Olson, 2011a: Response of precipitation extremes to idealized global warming in an aqua-planet climate model: towards a robust projection across different horizontal resolutions. *Tellus A*, **63 (5)**, 876–883.

Li, F., W. Collins, M. Wehner, D. Williamson, J. Olson, and C. Algieri, 2011b: Impact of horizontal resolution on simulation of precipitation extremes in an aqua-planet version of Community Atmospheric Model (CAM3). *Tellus A*, **63 (5)**, 884–892.

Lin, S.-J., 2004: A "vertically lagrangian" finite-volume dynamical core for global models. *Mon. Wea. Rev.*, **132 (10)**, 2293–2307, doi:10.1175/1520-0493(2004)132⟨2293:AVLFDC⟩2.0.CO;2, URL http://dx.doi.org/10.1175/1520-0493(2004)132<2293:AVLFDC>2.0.CO;2.

Lovejoy, S., D. Schertzer, and V. Allaire, 2008: The remarkable wide range spatial scaling of TRMM precipitation. *Atmos. Res.*, **90 (1)**, 10–32.

Mitchell, J. F. B., C. A. Wilson, and W. M. Cunnington, 1987: On CO_2 climate sensitivity and model dependence of results. *Quarterly J. Royal Met. Soc.*, **113 (475)**, 293–322, doi:10.1002/qj.49711347517, URL http://dx.doi.org/10.1002/qj.49711347517.

Moncrieff, M. W. and E. Klinker, 1997: Organized convective systems in the tropical western pacific as a process in general circulation models: A TOGA COARE case-study. *Q.J.R. Meteorol. Soc.*, **123 (540)**, 805–827, URL http://dx.doi.org/10.1002/qj.49712354002.

Morrison, H. and A. Gettelman, 2008: A new two-moment bulk stratiform cloud microphysics scheme in the community atmosphere model, version 3 (cam3). part i: Description and numerical tests. *J. Climate*, **21 (15)**, 3642–3659, URL http://dx.doi.org/10.1175/2008JCLI2105.1.

Murphy, J., D. Sexton, D. Barnett, G. Jones, M. Webb, M. Collins, and D. Stainforth, 2004: Quantification of modelling uncertainties in a large ensemble of climate change simulations. *Nature*, **430 (7001)**, 768–772.

Nastrom, G. and K. Gage, 1985: A climatology of atmospheric wavenumber spectra of wind and temperature observed by commercial aircraft. *J. Atmos. Sci.*, **42 (9)**, 950–960.

Neale, R., C. C. Chen, A. Gettelman, P. H. Lauritzen, S. Park, D. Williamson, et al., 2012: Description of the NCAR Community Atmosphere Model (CAM 5.0). *NCAR Technical Note, National Center of Atmospheric Research*, **TN-486+STR**.

Neale, R., et al., 2010: Description of the NCAR Community Atmosphere Model (CAM 4.0). *NCAR Technical Note, National Center of Atmospheric Research*, **TN-485+STR**.

Neale, R. B. and B. J. Hoskins, 2000: A standard test for AGCMs including their physical parametrizations: I: The proposal. *Atmosph. Sci. Lett.*, **1 (2)**, 101–107, doi:10.1006/asle.2000.0022, URL http://dx.doi.org/10.1006/asle.2000.0022.

Park, S., 2012: Toward a unified parameterization of convection across the scale-barrier, Abstract 1490378 presented at 2012 Fall Meeting, AGU, San Francisco, Calif. , 3–7 Dec.

Park, S., C. S. Bretherton, and P. J. Rasch, In Preparation: The revised cloud macrophysics in the community atmosphere model. *J. Climate*.

Platnick, S., M. King, S. Ackerman, W. Menzel, B. Baum, J. Riédi, and R. Frey, 2003: The MODIS cloud products: Algorithms and examples from Terra. *Geoscience*

and Remote Sensing, IEEE Transactions on, **41 (2)**, 459–473, doi:10.1109/TGRS.2002.808301, URL http://dx.doi.org/10.1109/TGRS.2002.808301.

Pressel, K. and W. Collins, 2012: First order structure function analysis of statistical scale invariance in the AIRS observed water vapor field. *J. Climate*, ***In Press*** **(2012)**.

Rasch, P. J. and J. E. Kristjánsson, 1998: A comparison of the CCM3 model climate using diagnosed and predicted condensate parameterizations. *J. Climate*, **11 (7)**, 1587–1614, URL http://dx.doi.org/10.1175/1520-0442(1998)011<1587:ACOTCM>2.0.CO;2.

Rauscher, S. A., T. Ringler, W. C. Skamarock, and A. A. Mirin, 2012: Exploring a global multi-resolution modeling approach using aquaplanet simulations. *J. Climate*, ***Accepted***.

Schumacher, C. and R. Houze, 2003: Stratiform rain in the tropics as seen by the TRMM precipitation radar. *J. Climate*, **16 (11)**, 1739–1756.

Skamarock, W., J. Klemp, M. Duda, L. Fowler, S. Park, and T. Ringler, 2012a: A multi-scale nonhydrostatic atmospheric model using centroidal Voronoi tesselations and C-grid staggering. *Monthly Weather Review*, ***Accepted*** **(2012)**.

Skamarock, W., J. Klemp, J. Dudhia, D. Gill, D. Barker, W. Wang, and J. Powers, 2005: A description of the advanced research WRF version 2. *NCAR Technical Note, National Center of Atmospheric Research*.

Skamarock, W. C., J. B. Klemp, M. G. Duda, L. D. Fowler, S.-H. Park, and T. D. Ringler, 2012b: A multiscale nonhydrostatic atmospheric model using centroidal Voronoi tesselations and C-grid staggering. *Mon. Wea. Rev.*, **140 (9)**, 3090–3105, URL http://dx.doi.org/10.1175/MWR-D-11-00215.1.

Stephens, G. L., et al., 2008: CloudSat mission: Performance and early science after the first year of operation. *J. Geophys. Res.*, **113 (D8)**, D00A18, doi:10.1029/2008JD009982, URL http://dx.doi.org/10.1029/2008JD009982.

Wilcox, E. M. and V. Ramanathan, 2001: Scale dependence of the thermodynamic forcing of tropical monsoon clouds: Results from TRMM observations. *J. Climate*, **14 (7)**, 1511–1524, URL http://dx.doi.org/10.1175/1520-0442(2001)014<1511:SDOTTF>2.0.CO;2.

Williamson, D., 2008: Convergence of aqua-planet simulations with increasing resolution in the Community Atmospheric Model, version 3. *Tellus A*, **60 (5)**, 848–862.

Williamson, D., 2012: Effect of time steps and time scales on parameterization suites. *Quarterly J. Royal Met. Soc.*, ***In Press***.

Wood, R. and P. R. Field, 2011: The distribution of cloud horizontal sizes. *J. Climate*, **24 (18)**, 4800–4816, URL http://dx.doi.org/10.1175/2011JCLI4056.1.

Yuan, T., 2011: Cloud macroscopic organization: order emerging from randomness. *Atmos. Chem. Phys.*, **11 (15)**, 7483–7490, URL http://www.atmos-chem-phys.net/11/7483/2011/.

Zhang, M., W. Lin, C. S. Bretherton, J. J. Hack, and P. J. Rasch, 2003: A modified formulation of fractional stratiform condensation rate in the NCAR Community Atmospheric Model (CAM2). *J. Geophys. Res.*, **108 (D1)**, 4035–4045, doi:10.1029/2002JD002523, URL http://dx.doi.org/10.1029/2002JD002523.